Numerical solution of the corona discharge problem based on mesh redefinition and test for a charge injection law

Bassem Khaddour, Pierre Atten, Jean-Louis Coulomb

*Published in J. Electrostatics, **66**, pp. 254-262 (2008)*

Numerical solution of the corona discharge problem based on mesh redefinition and test for a charge injection law.

B. Khaddour[1,2], P. Atten[1] and J.-L. Coulomb[2]

[1]Laboratoire d'Electrostatique et de Matériaux Diélectriques (LEMD), UMR 5517, UJF-CNRS, BP 166, 38042 Grenoble Cedex 9, France (e-mail: pierre.atten@grenoble.cnrs.fr)

[2] Laboratoire d'Electrotechnique de Grenoble (LEG), UMR 5529, INPG/UJF-CNRS, BP 46, 38402 Saint Martin d'Hères Cedex, France (e-mail: Jean-Louis.Coulomb@leg.ensieg.inpg.fr)

Abstract *- The paper presents a numerical and experimental study of corona discharge for a blade -plate configuration. Finite element method (FEM) is used to determine the electric potential between the electrodes and charge conservation equation is solved by the method of characteristics (MOC) to determine the charge density. The structured mesh is redefined at each step of the iterative scheme, the nodes of this structured mesh being the intersection points of the field and equipotential lines. The algorithm is applied for a simplified injection law at the blade. The numerical solutions give results which compare very favourably with experimental measurements of the characteristic curves I-V and of the current density distribution on the plate.*

Key word: Corona discharge, numerical modeling, eletric field, charge conservation equation, charge injection law.

1 Introduction

We consider the problem of injection of space charge ρ into an insulating gas through the corona effect. This space charge modifies the distribution of electrical field $\boldsymbol{E}$ which, in turn, controls the distribution of space charge. Corona discharges occur on electrodes with a small radius of curvature *r* (wire, needle tip, blade edge), where the electrical field takes very high values.

In the usual approach to obtain a numerical solution, the bi-ionized zone is neglected because its size is very limited compared with the electrode spacing. But disregarding the intricate phenomena occurring in the small discharge zone leaves us with the problem of prescribing the adequate condition for the ionic charge density. Here we use a so-called injection law which has proved to give a good approximation of the solution [1,2].

Most previous numerical models are not really general and satisfactory because they are limited to 2-D configurations with a wire as injecting electrode [3,4,5]. The boundary condition then is derived from the Kaptzov assumption [1,4] stating that the field on the discharging wire remains equal to the harmonic value it takes at the threshold voltage of corona discharge. In practice, in this case the electrical field at the injector is given by Peek law and the charge density on the wire is modified in the successive approximations approach until the computed field approximately takes the Peek value [3-5].

When the ionising electrode is not a wire (for instance, a needle or a blade), the electric field on the injecting electrode is far from being constant and it is necessary to distinguish the ionising and the non ionising zones. A few works for 3-D configurations [6-8] apply a generalized Kaptzov approximation by imposing a non zero charge density on the injecting electrode only in the region where the field exceeds the Peek value. Other ways of determining the charge density by considering the discharge phenomenon have also been considered [1]. There was also a particular approach modifying the charge density on the injecting electrode in order to obtain a computed current equal to the measured one [9]. For the problem considered here, we use the most satisfying boundary condition concerning the charge density on the injector, i.e. an injection law giving the charge density [1,2].

On another hand, the numerical methods used to determine the charge density are generally applied working with a structured mesh which remains unchanged during all the iterative computation. This introduces a numerical diffusion which can be most detrimental in the case of a needle or a blade as injecting electrode [8,9], because of the strong gradients in the charge distribution resulting from the peculiarities of corona discharges on such injecting electrodes. We focus here on a much more accurate numerical technique to solve the problem; this technique consists in redefining the mesh at each iteration step. When combined with a simple injection law, it gives solutions which fairly well correspond to the experimental observations.

2 Formulation of the problem

The two coupled equations, Poisson Eq. (1) and charge conservation Eq. (2), governing the electrical potential V and the charge density ρ of the injected ionic species in the drift zone are:

$$\nabla^2 V = -\rho/\varepsilon \tag{1}$$

$$\nabla.\boldsymbol{j} = 0 \tag{2}$$

where ε is the gas permittivity. The expression of the current density $\boldsymbol{j}$ is : $\boldsymbol{j} = \sigma \boldsymbol{E} + \rho(\boldsymbol{u} + K\boldsymbol{E}) - D\nabla\rho$, where D denotes the ions diffusion constant, $\boldsymbol{E} = -\nabla V$ the electrical field, σ the medium

conductivity, K the mobility of charge carriers and $\boldsymbol{u}$ the velocity field of the medium. In gases the medium conductivity is extremely small and we take $\sigma = 0$. The densities of diffusion current j_{diff} and convection current j_{conv} are negligible when compared with the drift current density j_{drift} [10]. Indeed, the orders of magnitude of the diffusion current density : $j_{diff} \sim D\,\rho/d$ and of the drift current density : $j_{drift} \sim K\,\rho\,V_{appl}/d$, combined with the Einstein relation $D/K = k_B T/e$ lead to :

$$\frac{j_{diff}}{j_{drift}} \sim \frac{k_B\,T}{e\,V_{appl}} \cong \frac{1}{40\;V_{appl}} \sim 10^{-6} \quad \text{for } T = 20°\text{C and } V_{appl} \sim 25\,\text{kV} \tag{3}$$

Here k_B is the Boltzmann constant, T the absolute temperature, e the elementary charge and V_{appl} the applied voltage. The order of magnitude of the convection current density is : $j_{conv} \sim \rho\,u_0$ where u_0 is the typical gas velocity ; a value of u_0 characterizing the gas convection induced by the Coulomb force acting on the space charge can be obtained by balancing the expressions of kinetic and electrostatic energy densities [10] : $(1/2)\,\varepsilon E^2 \sim (1/2)\,\rho_{gas}\,u_0^2 \Rightarrow u_0 \sim (\varepsilon/\rho_{gas})^{1/2}\,E$; we thus obtain (ρ_{gas} : gas density) :

$$\frac{j_{conv}}{j_{drift}} \sim \frac{u_0}{K\,E} \sim \frac{1}{K}\sqrt{\frac{\varepsilon}{\rho_{gas}}} \sim 10^{-2} \tag{4}$$

for air at atmospheric pressure. Therefore the current density expression simplifies into $\boldsymbol{j} = K\,\rho\,\boldsymbol{E}$. Then Eq. (2) writes $\nabla.(\rho\boldsymbol{E}) = \rho\nabla.\boldsymbol{E} + \boldsymbol{E}.\nabla\rho = 0$ and by using $\boldsymbol{E} = -\nabla V$ and relation (1) we obtain :

$$\boldsymbol{E}.\nabla\left(\frac{1}{\rho}\right) = \frac{1}{\varepsilon} \tag{5}$$

The boundary conditions associated with (1) are of Dirichlet type on the electrodes. Only one boundary condition concerning ρ can be associated with (2) : as justified in [1,2], the retained condition must prescribe the charge density at the injector. An injection law should be derived from an analysis of the bi-ionized zone. In practice, it is well known that the number of electrons and ions created by the ionizing electronic avalanches increases very dramatically with the field value E once E exceeds the threshold field E_{th} of corona discharge. It is the reason why Kaptzov formulated his assumption stating that, for an applied voltage V_{appl} above the threshold value V_{th} of corona discharge, the electrical field at the injecting electrode remains unchanged and equal to its harmonic value at V_{th} [1,3,4,7]. The simplest injection law compatible with the Kaptzov assumption and accounting for the observed phenomena is [2] :

$$\rho_{inj}(M) = \text{A}^*[E(M) - E_{th}] \quad \text{for} \quad E(M) > E_{th} \tag{6}$$

with A taking high values. This relation holds at every point *M* of the injecting electrode where the field *E(M)* is greater than the threshold field E_{th} for corona inception (ρ_{inj} (*M*) = 0 when *E(M)* < E_{th}).

We consider here the 2-D problem of a blade facing a plate, with the blade radius of curvature *r* being small compared with the distance *d* between blade and plate. The numerical study will be done in the domain limited by the two electrodes, the axis of symmetry and a field line of the harmonic solution taken as the outer boundary of the geometry (this outer field line is chosen far enough in order the solution in the charged zone be not perturbed by the approximation restricting the domain of integration [11,12]). We will work on the non dimensional equations :

$$\nabla^2 V = -\rho. \tag{7}$$

$$\boldsymbol{E}.\nabla\left(\frac{1}{\rho}\right) = 1 \tag{8}$$

The boundary conditions for the potential are $V_{blade} = 1$, $V_{plate} = 0$ and the Neumann condition $\partial V/\partial n = 0$ on the axis of symmetry and on the outer boundary [11,12]. The boundary condition for ρ is given by the injection law analogous to (6), where *A* is now a non dimensional constant and $A >> 1$.

3 Numerical methods

The two coupled equations (7) and (8) are solved, as usual, by successive approximations [2-12]. For a given ρ_k (distribution of ρ at the iteration step *k*), the new potential V_{k+1} is obtained by solving Eq. (7). With the new field distribution, solving Eq. (8) gives a charge density distribution ρ'_{k+1}. For low enough injection level, we can take $\rho_{k+1} = \rho'_{k+1}$, but for strong injection, in order to avoid instability during the iteration, it is necessary to use an under-relaxation procedure with the parameter *w* such that $0 < w \leq 1$ [2,9-12] :

$$\rho_{k+1} = (1-w)\rho_k + w\,\rho'_{k+1} \tag{9}$$

A structured mesh was used whose nodes are the intersection points of selected electrical field lines and equipotential lines (Fig. 1). The potential distribution *V* is determined by solving Poisson equation (7) with the finite element method (FEM) of first order applied on the triangular structured mesh [10-12]; the triangles are obtained by dividing the quadrangles which are formed by the intersecting electrical field and equipotential lines (Fig. 1).

Two methods were tested to solve the charge conservation equation, the finite volume method (FVM) and the method of characteristics (MOC). The FVM (applied on the form $\nabla.(\rho\boldsymbol{E}) = 0$ of the charge conservation equation) always gives a local minimum of the charge density on the symmetry axis [10,11]. When working on a fixed mesh (i.e. not changed during the iterative

scheme), the solution is close to the one obtained by using the MOC and exhibits the same smoothing of ρ at the lateral boundaries of the space charge zone. Moreover, when redefining the mesh at each iteration step (as it is explained below), the FVM is very sensitive to the mesh changes and this makes it necessary to take a very small value of the under-relaxation factor *w*.

The second technique to solve (8) is the method of characteristics (MOC) which is well suited for hyperbolic equations and has been used extensively in the space charge problem [1-3,8,10-12]. In this method, we follow the charge along a field line from an initial point on the blade up to the plate. In order to illustrate the phenomenon of numerical diffusion occurring when discretizing (8) on a fixed structured mesh, let us consider the simplified case depicted on Fig. 2 (rectangle with local *Ox* and *Oy* axes). The charge carriers leave the point M_0 and drift along the characteristic line to the point *M*; during this movement the space charge density is affected by the field $\boldsymbol{E}$ and by space charge self-repulsion. By discretizing (8) on the segment M_0M (see Fig. 2), we obtain :

$$\frac{1}{\rho_M} = \frac{1}{\rho_{M_0}} + \frac{D_{PM}}{E_x} \tag{10}$$

where D_{PM} is the distance between points P and M and E_x is the *x*-component of the field. The linear interpolation of the function $1/\rho$ between points P and T leads to the following expression (formulation MC1) with an adequate factor α [10] :

$$\frac{1}{\rho_M} = (1-\alpha)\left(\frac{1}{\rho_P}\right) + \alpha\left(\frac{1}{\rho_T}\right) + \frac{D_{PM}}{E_x} \tag{11}$$

We consider the most difficult problem of a rectangular distribution of injected charge on the blade : $\rho_{inj} = \rho_{max} \neq 0$ for the curvilinear abscissa $s < \lambda$ and $\rho_{inj} = 0$ for $s > \lambda$, λ characterizing the width of the ionising zone on the blade. In the case $\rho_T > 0$ and $\rho_P = 0$, we obtain $\rho_M = 0$ from (11). This means that the computed charged zone is restricted by a particular field line of the harmonic solution as sketched by Fig. 3 (this field line will not change during the iterative procedure). This of course results in the corona current between blade and plate not being conserved and in the absence of spreading of the space charge (a better treatment would be to determine the separatrix between charged and charge free zones and, hence, to refine the discretization scheme). We tried another way by making an interpolation – the corresponding scheme is denoted MC2 – on the function ρ instead of $1/\rho$ [10,11] :

$$\frac{1}{\rho_M} = \frac{1}{(1-\alpha)\,\rho_P + \alpha\,\rho_T} + \frac{D_{PM}}{E_x} \tag{12}$$

With this formula we have now $\rho_M \neq 0$ and it is found that the corona current is well conserved [11]. But the width of the charged zone is larger than the real one (see the continuous field line

delineating the real charge zone on Fig. 3) and it is easy to see that the distribution of charge density is smoothed and looks similar to the one which would exist with a strong diffusion effect. It is the reason why we call “numerical diffusion” this effect of smoothing of strong lateral gradients induced by the approximations made in the discretization scheme.

Most approaches to solve the problem of space charge injected by corona discharge are using discretization schemes which introduce such a numerical diffusion. Only one previously published method is correct and does not introduce a numerical diffusion [8]. This method consists in solving the Poisson equation by the FEM, always on the same structured mesh, but determining the charge density distribution by drawing a great number of characteristic lines and calculating ρ’ at numerous nodes on these characteristic lines (provisional mesh) ; the charge density at the nodes of the FEM mesh is then obtained by interpolation from the values of ρ at the nodes of the provisional mesh [8]. This algorithm eliminates the numerical diffusion but it requires a great number of provisional nodes and a long computation time to obtain the solution.

We proposed a different approach [10-12] with an adaptive mesh. At every iteration step, once a new potential distribution V_{k+1} has been determined, a new mesh is defined whose nodes are the intersections of the field lines and equipotential lines relative to V_{k+1}. In this way solving eq. (8) is elementary because (8) on the field lines reduces to an ordinary differential equation. For successive nodes lying on a same field line, referring to Fig. 2, we simply have :

$$\frac{1}{\rho_M} = \frac{1}{\rho_P} + \frac{D_{PM}}{E} \qquad \text{with} \qquad E = \frac{V_P - V_M}{D_{PM}} \tag{13}$$

4 Mesh redefinition

The technique of mesh redefinition was first developed in the case of a well defined charge density distribution ρ_{inj} on the blade. The first key point in the procedure is to determine the field lines. By using the linear representation of the potential in the triangles of the FEM mesh, difficulties are faced because of the discontinuous character of the associated field distribution. To illustrate these difficulties, let us consider first the problem when keeping unchanged the nodes on the blade which are the starting points of the new field lines to be determined. Each starting node belongs to 3 triangles of the former mesh and we should make a choice between the 3 possible fields. Other difficulties induced by the discontinuity of electrical field also arise when the new field line crosses a lateral side between two triangles; all attempts to overcome these difficulties did not prevent the algorithm from diverging. In order to have a smoother field distribution, we worked on quadrangles. In practice, a local value of the field was derived from a linear representation of the potential on two laterally adjacent quadrangles using a weighted least square formulation [10] (the

weight of each of the six nodes is a function of the distance between the node and the field line). Once the new field lines are determined, the new nodes on them are obtained from prescribed values of the electric potential [10]. In this way the algorithm converges and gives reasonable approximate solutions provided the level of injected space charge is moderate enough ($\rho_{max} < 10$). In the case $\rho_{max} > 10$, after a limited number of iterations (8 to 20 depending also on w), the field lines tend to accumulate near the boundary of the charged zone because of the strong divergence of the field lines in the zone of high space charge (Fig. 4) and the algorithm diverges [11].

We therefore turned towards the redefinition of the nodes on the blade which constitutes the second key point of the procedure of mesh redefinition. This operation is not easy because the stability and convergence of the whole algorithm are very sensitive to the nodes distribution on the blade. In order to obtain a mesh which is both sufficiently regular and refined enough in the vicinity of the blade edge, we imposed the condition that the field lines arrive very close to the arrival points of the harmonic field lines (initial mesh) on the plate. A procedure was developed (including an under-relaxation and severe bounds) to have a very progressive evolution of the set of nodes on the blade (and hence in the whole domain) [10].

The convergence to the numerical solution is then slow and the under-relaxation (9) between two successive approximations of the charge density distribution must be moderated (14). In practice for strong injection as it is the case when using the injection law, the following expression was used for the interpolation factor w_k :

$$w_k = w_0 \tanh\left(\frac{k}{n_{relax}}\right) \tag{14}$$

where k is the iteration number, w_0 is the maximum value (typically $w_0 \sim 0.1$) and n_{relax} is a constant ranging from 20 to 50. A suitable choice of the initial mesh, of the two under-relaxation factors and other parameters leads to a good convergence [10] : the mean difference $\delta\rho_m$ between two successive approximations of ρ becomes lower than 10^{-6} after 80 to 100 iterations for a given (strong) distribution ρ_{inj} on the blade and a limited total number of nodes ($N_{total} \sim 1200$). A criterion to evaluate the degree of approximation of the numerical solution is the conservation of total current from one electrode to the other. The relative difference between the currents calculated on the two electrodes is lower than 0.02 in the case $N_{total} \sim 1200$ and decreases with N_{total}.

5 Some numerical results

The algorithm based on FEM, MOC and mesh redefinition as described in the preceding sections has been applied to determine the solutions when using the injection law (6). Because of the stabilizing nature of the interplay between E and ρ , the use of (6) does not basically modify the

conditions of convergence of the iterative numerical scheme and only an adjustment of the various parameters is required. Typically, in the case of a thin blade ($r/d \sim 0.015$), for A values ≥ 50, about 120 iterations are sufficient to obtain a good convergence (mean difference $\delta\rho_m \leq 10^{-4}$).

Fig. 5-a shows the field lines obtained in the particular case $r/d \cong 0.012$, $V_{appl}/V_{th} = 1.4$ and A = 100. In the charged zone close enough to the blade edge, the curvature of the field lines is positive and opposite to the curvature of the harmonic field lines. This is due to the strong space charge effect in this region (Coulomb repulsion). We can see on the strongly magnified picture around the blade edge (Fig. 5-b) that the redefinition of the nodes on the blade finally leads to field lines very close to each other in the injecting zone and much more distant on the blade section without injection. We also see that the injection is restricted to a very narrow part on the hemi cylindrical edge of the blade (Fig. 5-b).

The current-voltage characteristic curves obtained when using the injection law (6) are shown on Fig. 6 for 3 values of the parameter A. These curves have a shape fully similar with the one of the measured characteristics and the comparison presented in the next section will show the very good adequacy of the retained injection law to account for the experimental results. We also note from Fig. 6 that the parameter A has a very small influence on the prediction of the total current *I*.

The distributions of electric field and charge density at the blade are a little more sensitive on the A value. Close to the symmetry axis, from (6) it is clear that, to a rough approximation, the difference $E - E_{th}$ is inversely proportional to A (Fig. 7-a); this figure also shows that for an applied voltage at least two times greater than the inception voltage of corona discharge, the field *E* takes nearly constant values in the injecting zone. The influence of A is most noticeable on the distributions of injected charge density ρ_{inj} ; there is a small increase with A of the maximum ρ_{inj} value; Fig. 7-b shows that the ρ_{inj} distribution tends to become more and more flat when A is increased with a more and more marked decrease, thus suggesting a shape evolution toward a rectangular profile as $A \rightarrow \infty$.

Fig. 8 shows the distribution of current density *J* on the collecting plate (the corresponding dimensional variable is in A/m). The parameter A has a limited influence on these calculated *J* distributions, *J* slightly increasing when A is increased; but as the width of the charged zone slightly decreases, the total current calculated on the plate has a very limited increase with A (see Fig. 6). The strong gradient in the injected charge density distribution on the blade is well conserved in the charge and current distributions on the plate. The curves of Fig. 8 clearly show that the *J* maximum value and the width of the charged zone increase when the applied voltage is increased.

6 Experimental Study

An experimental study has been performed in order to compare the computed solutions with measurements. In most of the previous studies, the authors tested their numerical solutions by comparing the current-voltage characteristics only. This is not a really valuable test because the current is a global variable which can hide strong departures in the distributions of field and charge density. Here we intend to compare variables related with the charge density distribution ρ. The simplest way to obtain information on ρ is to examine the current density on the plate.

We used a simple test set-up (Fig. 9) with a blade of length ≅ 35 cm and thickness e_{blade} = 0.3 mm, rounded at the edge in order to have a shape as close as possible to a hemi cylinder (radius of curvature r = 0.15 mm). The collecting plate has been cut in two parts between which thin metallic foils were inserted (Fig. 9). The central small elongated electrode, insulated from the two halves of the plate, is parallel to the blade and its effective area is 12 mm × 0.6 mm (within a few percent). The current i captured by this small electrode enables to obtain a very good approximation of the current density on the plate because the width of this thin electrode is small compared with the distance d (Fig. 9). The measurement of the current density distribution on the plate was made easy through the use of a translation table moving the blade parallel to the plate (at constant distance d) and in the direction normal to the blade.

For negative polarity of the blade, the corona discharge is inhomogeneous and unstable along the blade edge (tuft corona). It is the reason why the study was carried out with corona discharge of positive polarity. The characteristic curves I-V were measured for different values of the distance d (Fig. 10). We can determine the corona inception voltage V_{th} from these curves : V_{th} ≅ 20.4 kV for d = 2.45 cm, V_{th} ≅ 18.7 kV for d = 1.8 cm and V_{th} ≅ 15.5 kV for d = 1.2 cm. Note that the mean electrical field could take values up to 20 kV/cm, a rather high value in air at atmospheric pressure. As it is well known, several physical parameters influence the corona discharge in atmospheric air : temperature, pressure, humidity. We observed that the slope of the curves I/V = f(V), proportional to the ions mobility, as well as the inception voltage V_{th} varied from one day to another day. By comparing the results obtained during different days, we concluded that the mobility K of charge carriers could vary by up to about 10% depending on the environment parameters. Therefore all necessary measurements corresponding to a given value of the distance were carried out in the shortest possible time.

Fig. 11 shows typical variations of the measured current i captured by the small electrode as a function of the normalized abscissa x/d on the plate. The profiles of Fig. 11 exhibit a good symmetry as expected. The charged zone is well determined by the current density on the plate

which is zero outside this charged zone. From Fig. 11, it is clear that the width of the space charge zone on the plate increases with the applied voltage but takes limited values ($\leq d$); this indicates that the width of the injecting zone on the blade edge is very restricted. We also note on the profiles a steep decrease of the current down to zero at a certain distance (the smoothing is partly due to the finite width of the measuring electrode). This steep decrease is the image of the quasi-discontinuity of the charge injection intensity on the blade. Finally, by comparing with similar current density profiles obtained in the needle-plate configuration, it appears that in the blade-plate case, the space charge does not spread largely and the current density does not exhibit a Warburg-like distribution.

7 Comparison with computed solutions

Qualitatively, the numerical results are very similar to the measurements as concerns the I-V curves (see Figs. 6 and 10) and the current density profiles on the plate (see Figs. 8 and 11). In order to have quantitative comparisons, numerical solutions were determined for this configuration of a blade with cylindrical edge (radius of curvature r = 0.15 mm) facing the plate (at distance d) by using the technique of mesh redefinition as described in §4. Several parameters involved in the mesh redefinition had to be adequately adjusted to take into account the effect of the blade thinness.

For the first measured distance d =1.2 cm, the variations of the measured ratio I/V_{appl} as a function of V_{appl} give a nearly perfect straight line (Fig. 12) in the limited range of applied voltage [V_{th}, 1.6 V_{th}]. The computed current values also exhibit a very linear variation (Fig. 12). The very good agreement between the measured and computed results has been obtained here by retaining for the mobility of positive charge carriers the value $K = 2.1\ 10^{-4}$ m^2/V.s which is quite similar to the published values of mobility of positive ions generated by corona discharge in air. For the second measured distance (d =1.8 cm) we obtained again a very good agreement between computed and measured values of I/V with a slightly different mobility value $K = 2.03\ 10^{-4}$ m^2/V.s. This agreement gives a first test for the validity of the injection law used in the numerical modelling.

The second test concerns the current density on the plate which is a much more sensitive variable. Figs. 13 and 14 show that the measured values of the current density (made non dimensional by using in particular the above determinations of K), agree reasonably well with the computed ones. The shapes are similar and exhibit a steep decrease at the boundary of the charged zone. The difference in the zones of steep decrease arises partly from the width e_{probe} of the small probe electrode which would convert a real discontinuity of current density into a linear decrease over a narrow interval of width e_{probe}. The width of space charge zone appears to be fairly well predicted by numerical calculations. The level of J in the central zone is also very well predicted by the computation in the case of applied voltage V_{appl} moderately above V_{th} (Figs. 13 and 14).

There are nevertheless some differences in the shape of calculated and measured current density curves.. The characteristic width of the zone of strong decrease of the measured J (between ≅ 0.05 and 0.1) is clearly larger than the electrode width e_{probe} and, very likely, this arises from the equivalent distribution on the blade induced by the corona discharge. Otherwise, for V_{appl} values significantly higher than V_{th}, the shape of measured current density is more acute than the computed one. This might partly arise from the shape of the blade edge which probably differs from the perfect hemi cylinder retained in the numerical model. But there is another possible reason for the obtained shape : with positive corona discharge there is a marked tendency to induce intermittent streamers of limited length; the bi-ionised zone of discharge should then induce a deformation of the time averaged field and a kind of extension of the electrode, thus resulting in the rather acute current density profiles as visible on Fig. 11 for V_{appl} above about 23 kV.

8 Conclusions

The numerical code using the techniques MOC and FEM with redefinition of the structured mesh defines an algorithm which converges well and gives the solution of the problem of the field modified by an injected space charge. The mesh redefinition is very interesting because the solutions can exhibit strong lateral gradients of space charge; moreover this technique gives immediately the equipotential and field lines.

We have proposed a simplified injection law which is qualitatively well justified for corona discharge on electrodes other than wires and which leads to solutions looking very similar to the observations. In the particular configuration of a thin blade facing a plate, with the retained injection law, the algorithm gives solutions which very satisfactorily predict the variations of the total current and the profiles of current density on the plate as measured for a positive corona discharge on the blade.

The particular technique of mesh redefinition should be extended without major difficulty to axisymmetrical configurations like the so-called point-plane electrodes system. The generalization of the algorithm to real three-dimensional electrode configurations would be very interesting for several applications, but this generalization is far from being straightforward and requires detailed investigations.

References

[1] K. Adamiak, V.Atrazhev and P.Atten , “Corona discharge in the hyperbolic point-plane configuration: direct ionization criterion versus approximate formulations”, IEEE Trans. Diel. & Electr. Insul., Vol. 12, No. 5; October 2005, pp. 1025-1033.

[2] P. Atten, K. Adamiak, Bassem Khaddour and J.-L. Coulomb, “Simulation of corona discharge in configurations with a sharp electrode”. J. Optoelectron. Adv. Mater., 6 (3), 2004, pp. 1023-1028.

[3] J.L. Davis and J. F. Hoburg, **“**Wire-duct precipitator field and charge computation using finite element and characteristic method**”,** J. Electrostatics Vol. 14, (1983), pp.187-199.

[4] S. Cristina, G. Dinelli, and M. Feliziani, “Numerical computation of corona space charge and V-I characteristic in DC electrostatic precipitators”, IEEE Trans. Ind. Appl., Vol. IA27, No. 1, (1991), pp. 147-153.

[5] A.J. Medlin, C.A.J Fletcher and R. Morrow, “A pseudotransient approach to steady state solution of electric field-space charge coupled problems”. J. Electrostatics, Vol. 43, (1998), pp. 61-77.

[6] J.H. Davidson, P.J. McKinney and P. Linnebur, “Three-dimensional (3-D) model of electric field and space charge in the barbed plate-to-plate precipitator“, IEEE Trans. Ind. Appl., Vol. IA32, (1996), pp. 858-866.

[7] A.M. Meroth, T. Gerber, C.D. Munz, P.L Levin and A.J. Schwab, “Numerical solution of non stationary charge coupled problems”, J. Electrostatics, 45 (1999), pp. 177-198.

[8] K. Adamiak and P. Atten, “Simulation of discharge corona in point-plane configuration”, J. Electrostatics, 61 (2004), pp. 85-98.

[9] A.A Elmoursi and C.E Speck, “Simulation of space charge in unbounded geometries“, IEEE Trans. Ind. Appl., Vol. IA26, (1990), pp. 384-392.

[10] B. Khaddour, “Modélisation du champ électrique modifié par la charge d’espace injectée“, Ph. D. thesis, Institut National Polytechnique de Grenoble (INPG), France (21 November 2006).

[11] P. Atten, J.-L. Coulomb and B. Khaddour, “Modeling of electrical field modified by injected space charge”, IEEE Trans. Magnetics, Vol. 41, No 5, (2005), pp. 1436-1439.

[12] B. Khaddour, P. Atten and J.-L. Coulomb, "Electrical field modified by injected space charge in blade-plate configuration", IEEE Trans. Magnetics, Vol. 42, No. 4, (2006), pp. 651-665.

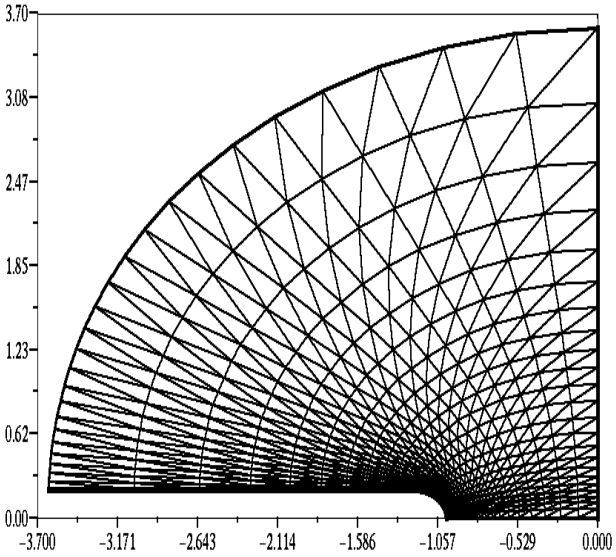

Fig.1 – Initial structured mesh for the blade-plate configuration (r = 0.2).

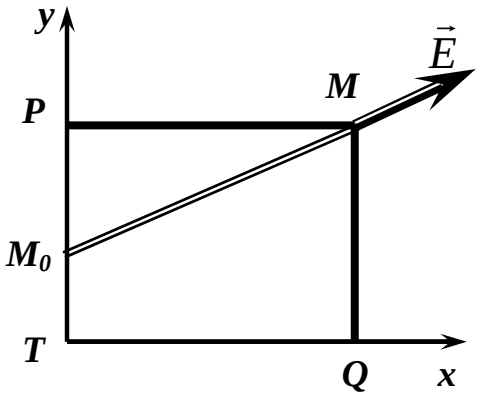

Fig. 2 – Characteristic line and MOC application.

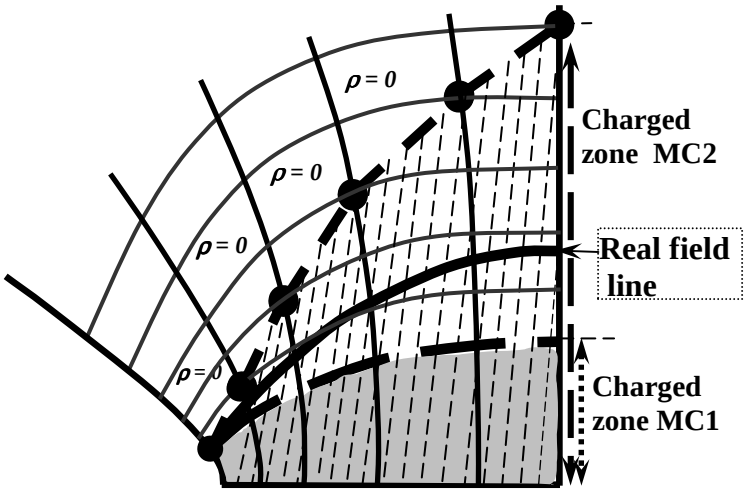

Fig. 3 – Real field line separating the charged and charge free zones and the approximations corresponding to MC1 and MC2.

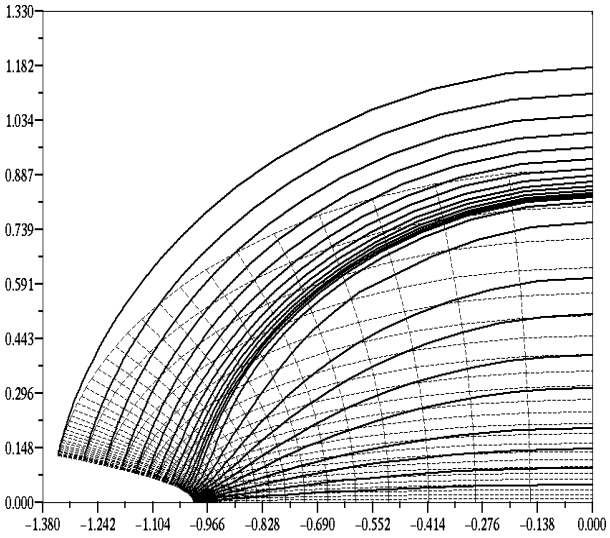

Fig. 4 – Field lines (in the central part of the geometrical domain) obtained at iteration #8 in the case of a rectangular distribution of injected charge (ρ_{max} = 25) by using always the same nodes on the (hyperbolic) blade (r/d = 0.02, $N_x = N_y$ = 35).

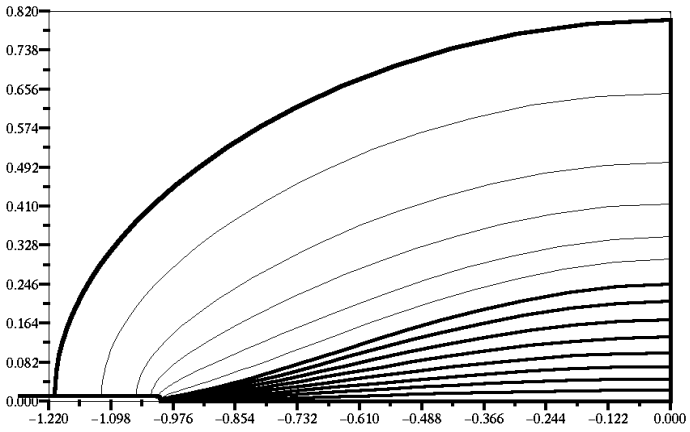

(*a*)

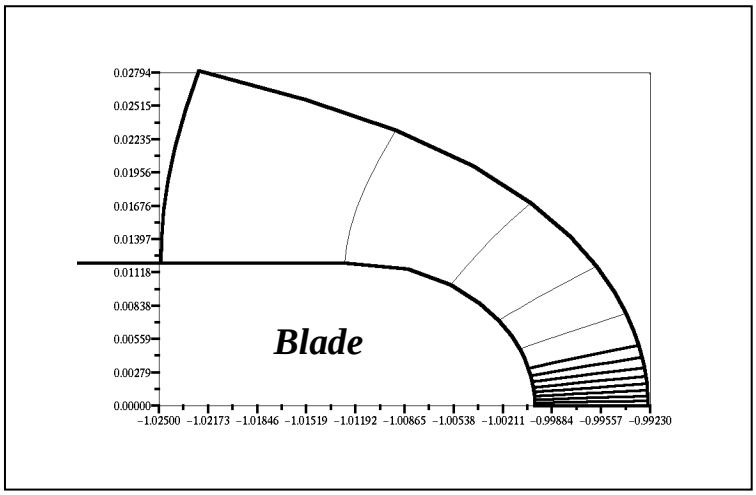

(*b*)

Fig.5 – Solution for the thin blade ($r/d \cong 0.012$ - d = 1.2 cm) taking the value A = 100 in the injection law (5) (mesh with $N_x = N_y = 35$). Field lines in the charged zone (thick lines) and in the charge free zone (thin lines). a) field lines pattern in the central part of the domain; b) highly magnified picture around the blade edge.

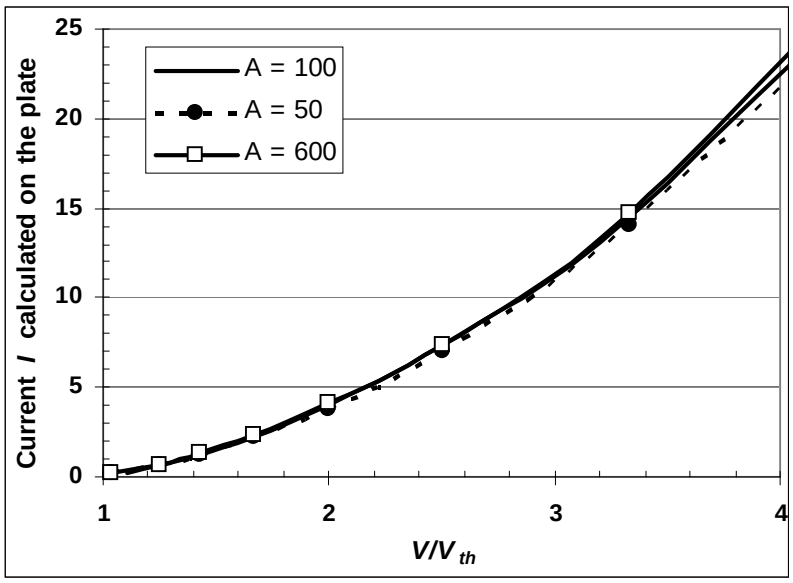

Fig. 6 – Normalized characteristic I-V, for a thin blade (r/d = 0.01), calculated for several values of the parameter A of the injection law (5) ($N_x = N_y = 35$).

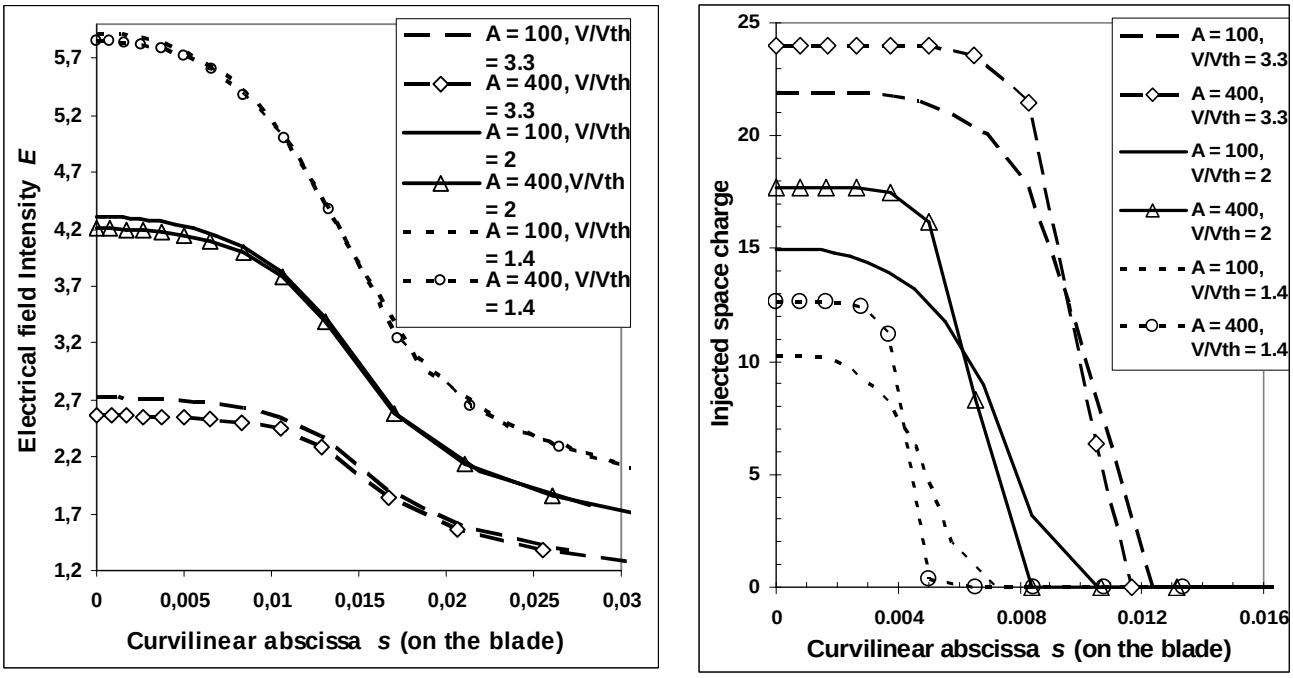

Fig. 7 – Variations versus the curvilinear abscissa s on a thin blade (r/d = 0.01) of: a) the (non dimensional) field intensity E; b) the (non dimensional) charge density ρ_{inj}.

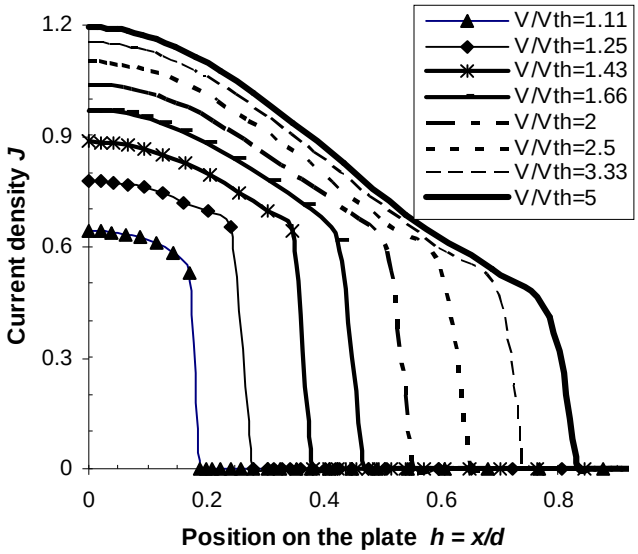

Fig. 8 – Current density distribution on the plate $J = f(h)$ for a thin blade (r/d = 0.01) calculated for A = 100 ($N_x = N_y = 35$).

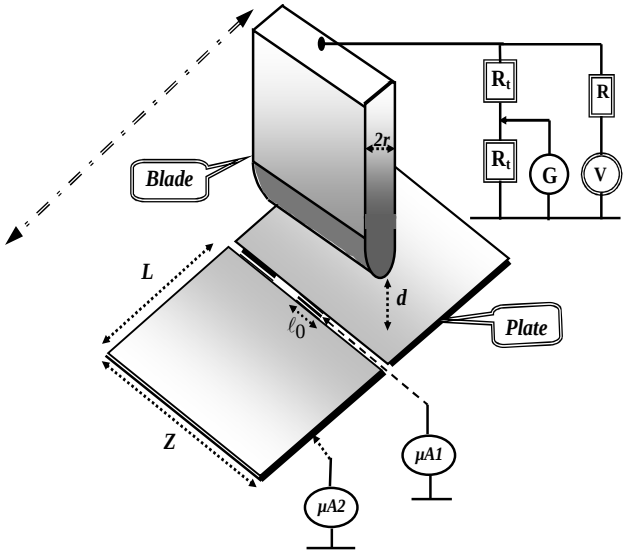

Fig. 9 – Schematic view of the blade-plate experimental configuration.

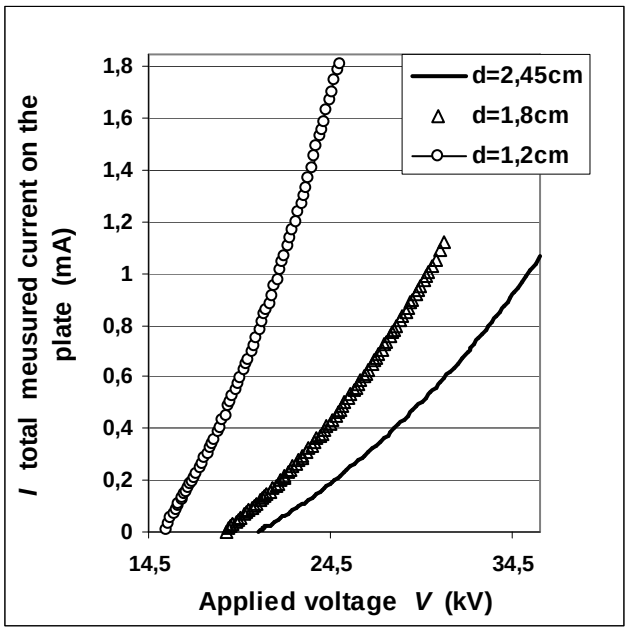

Fig. 10 – Variations of the current I as a function of the applied voltage V for 3 values of the distance d (r = 0.15 mm).

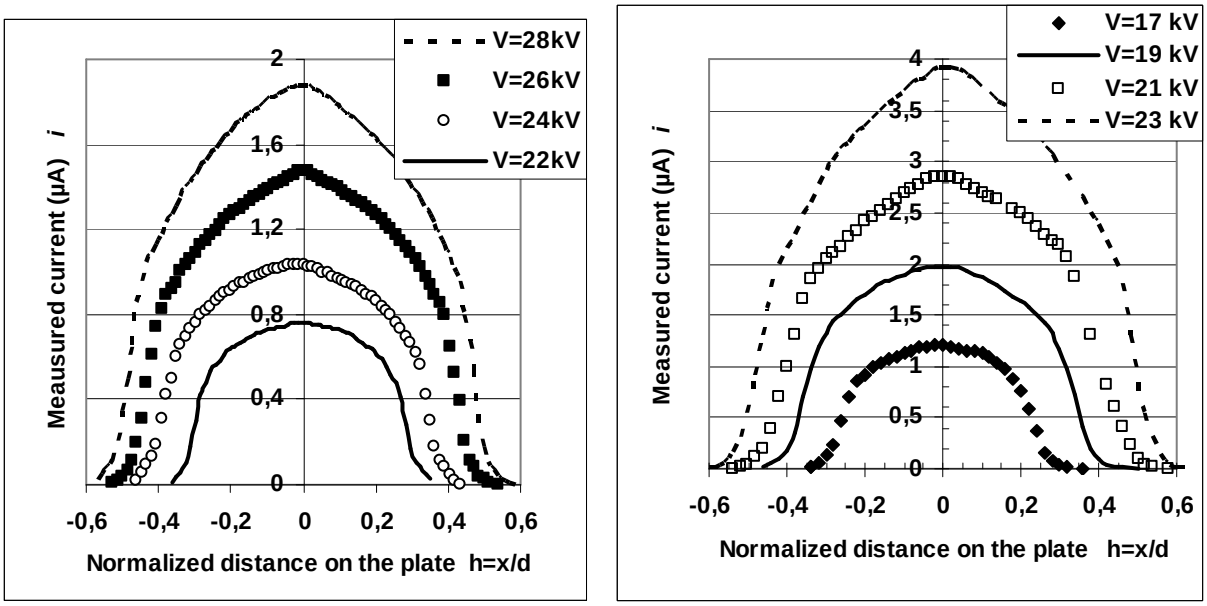

(a) **(b)**

Fig. 11 – Variations versus probe electrode position of the current *i* captured by the probe electrode a) $d = 1.8$ cm; b) $d = 1.2$ cm.

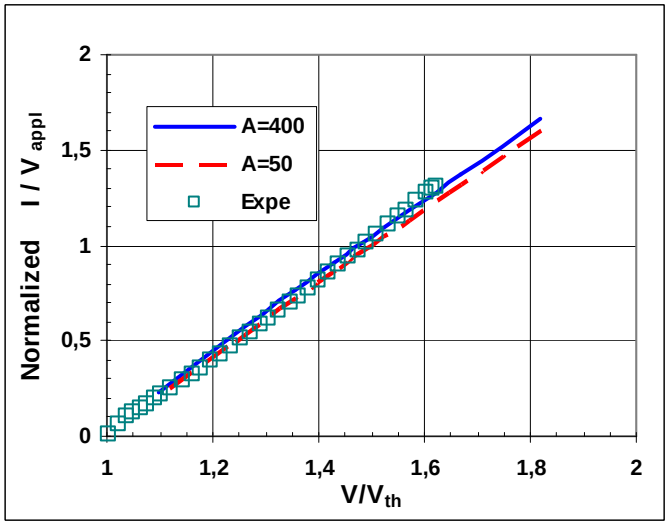

Fig. 12 – Numerical and experimental non dimensional values of I/V_{appl} versus V_{appl}/V_{th} (d = 1.2 cm).

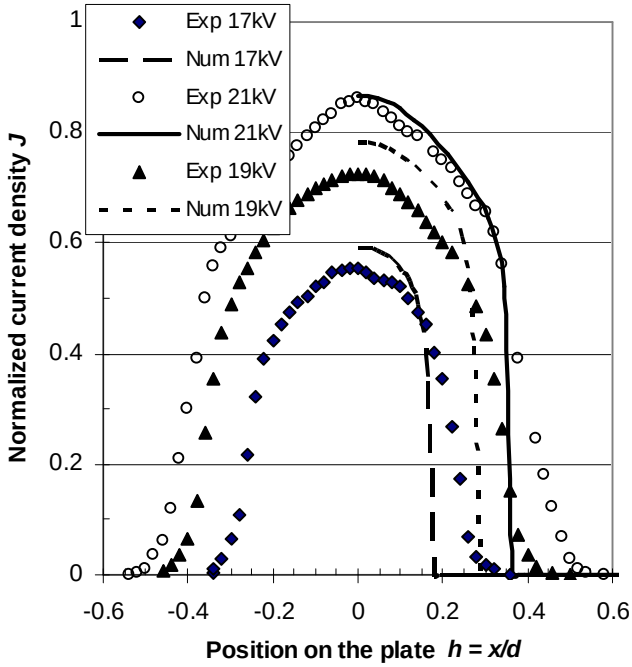

Fig. 13 – Comparison of numerical and experimental non dimensional current densities on the plate in the case d = 1.2 cm.

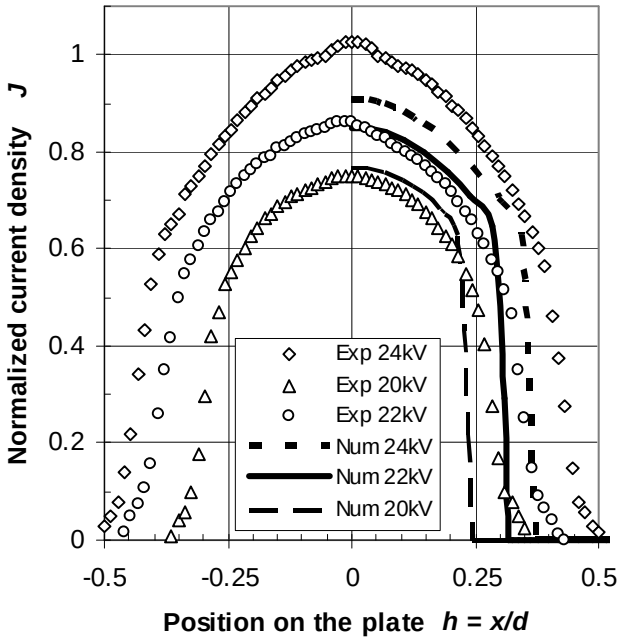

Fig. 14– Comparison of numerical and experimental non dimensional current densities on the plate in the case d = 1.8 cm.